HHS Public Access

Author manuscript

Nat Immunol. Author manuscript; available in PMC 2012 May 01.

Published in final edited form as:

Nat Immunol. 2011 November ; 12(11): 1045–1054. doi:10.1031/ni.2131.

Innate lymphoid cells promote lung tissue homeostasis following acute influenza virus infection

Laurel A. Monticelli[1,2], **Gregory F. Sonnenberg**[1,2], **Michael C. Abt**[1,2], **Theresa Alenghat**[1,2], **Carly G.K. Ziegler**[1], **Travis A. Doering**[1], **Jill M. Angelosanto**[1], **Brian J. Laidlaw**[1], **Cliff Y. Yang**[3], **Taheri Sathaliyawala**[4], **Masaru Kubota**[4], **Damian Turner**[4], **Joshua M. Diamond**[5], **Ananda W. Goldrath**[3], **Donna L. Farber**[4], **Ronald G. Collman**[5], **E. John Wherry**[1], and **David Artis**[1,2]

[1]Department of Microbiology and Institute for Immunology, Perelman School of Medicine, University of Pennsylvania, Philadelphia, PA 19104, USA

[2]Department of Pathobiology, School of Veterinary Medicine, University of Pennsylvania, Philadelphia, PA 19104, USA

[3]Department of Biology, University of California San Diego, La Jolla, CA 92037, USA

[4]Department of Surgery and the Columbia Center for Translational Immunology, Columbia University Medical Center, New York, NY 10032, USA

[5]Department of Medicine, School of Medicine, University of Pennsylvania, Philadelphia, PA 19104, USA

Abstract

Innate lymphoid cells (ILCs), a recently identified heterogeneous cell population, are critical in orchestrating immunity and inflammation in the intestine but whether ILCs can influence immune responses or tissue homeostasis at other mucosal sites remains poorly characterized. Here we identify a population of lung-resident ILCs in mice and humans that expressed CD90, CD25, CD127 and T1-ST2. Strikingly, mouse ILCs accumulated in the lung following influenza virus infection and depletion of ILCs resulted in loss of airway epithelial integrity, decreased lung function and impaired airway remodeling. These defects could be restored by administration of the lung ILC product amphiregulin. Collectively, these results demonstrate a critical role for lung ILCs in restoring airway epithelial integrity and tissue homeostasis following influenza virus infection.

Correspondence should be addressed to D.A. (dartis@mail.med.upenn.edu) or E.J.W. (wherry@mail.med.upenn.edu).

Author Contributions

L.A.M., G.F.S. and M.C.A. performed experiments and analyzed data. T.A. analyzed lung histological specimens. C.G.K.Z. and T.A.D. performed microarray analysis. J.M.A. and B.J.L. designed influenza virus qRT-PCR quantification method. C.Y.Y. and A.W.G. generated and provided Id2-deficient fetal liver chimeras. T.S., M.K., D.T. and D.L.F. collected and processed human lung tissue. J.M.D. and R.G.C collected and processed human BAL fluid. L.A.M., E.J.W. and D.A. designed the study, analyzed experiments, and wrote the manuscript.

Introduction

Maintenance of epithelial barrier function at mucosal sites such as the intestine and respiratory tract is critical to limit exposure to environmental stimuli, commensal bacteria and invading pathogens[1–3]. Recent studies have highlighted multiple roles for innate lymphoid cells (ILCs) in regulating immunity and/or inflammation at the intestinal barrier[4,5]. ILCs are a diverse family of immune cells that are heterogeneous in their tissue location, cytokine production and effector functions[4,5]. Although the lineage relationships between these heterogeneous ILC populations remain poorly understood, they are hypothesized to originate from a common Id2-dependent progenitor cell[4,6]. Based on their differential expression of RORγt, mouse ILCs can be functionally divided into at least two populations. RORγt-positive ILCs include $CD4^+$ lymphoid tissue inducer (LTi) cells, $NKp46^+$ ILCs and a population of $CD4^-$ $NKp46^-$ ILCs, all of which express interleukin 17A (IL-17A) and/or IL-22 and can promote intestinal immunity and/or inflammation[4,7–10]. A second group of RORγt-negative ILCs express the T_H2 cell-associated cytokines IL-4, IL-5 and IL-13, and are composed of nuocytes, natural helper cells (NHCs), innate helper type 2 cells (Ih2) and multi-potent progenitor type 2 cells (MPP^{type2}). These cells are activated in response to the epithelial cell-derived cytokines IL-25 and/or IL-33 and can promote T_H2 cytokine-dependent protective immunity against helminth parasites[11–14].

Although these phenotypically distinct ILC populations have been identified in intestinal and lymphoid tissue compartments of mice, whether ILCs are present at barrier surfaces in humans and whether they influence immune responses or tissue homeostasis at extra-intestinal sites remains unclear. Recent work has identified a population of ILCs in the lungs of mice that resembled NHCs and nuocytes in phenotype and cytokine expression profile[15]. Following exposure to high-dose H3N1 influenza virus, these lung ILCs promoted airway hyperreactivity early following infection via an IL-13-dependent mechanism. However, the potential influence of lung ILCs on other aspects of immunity, inflammation or tissue repair and remodeling in the respiratory tract remains unknown.

The repair and remodeling of damaged or inflamed tissue is a complex process involving many factors, including cytokines, chemokines, growth factors and extracellular matrix proteins that restore tissue homeostasis after injury[16,17]. Tissue remodeling following acute injury requires a balance between promoting beneficial repair responses that drive cell proliferation while also acting to limit these responses once the tissue has been adequately remodeled[16,17]. Failure to either appropriately initiate or resolve these repair responses can have detrimental effects, including loss of tissue integrity or function and promotion of chronic inflammation or tissue fibrosis[16,17]. The cellular and molecular regulators of tissue remodeling following injury or infection at mucosal tissues such as the lung are not well understood.

In this study, we employ infection with the H1N1 PR8 strain of influenza virus and identify a previously unrecognized role for ILCs in promoting restoration of tissue homeostasis in the lung. In mice, lung-resident ILCs were Lin^- and expressed cell surface markers associated with NHC populations, including CD90, CD25, CD127 and T1-ST2 and produced IL-5 and IL-13 in response to IL-33 stimulation. An analogous population of Lin^-

lung ILCs was also present in bronchoalveolar lavage fluid and lung parenchyma of humans. ILCs accumulated in the lung of wild-type (WT) or *Rag1*$^{-/-}$ mice following experimental influenza virus infection and depletion of CD90^{+} ILCs or blockade of IL-33-IL-33R signaling in influenza virus-infected mice resulted in severely decreased lung function, loss of airway epithelial integrity and impaired respiratory tissue remodeling. Genome-wide transcriptional profiling of lung ILCs identified a strong enrichment for genes that regulate wound-healing processes, including the epidermal growth factor family member amphiregulin. Amphiregulin restored lung function and promoted tissue remodeling in ILC-depleted influenza virus-infected mice. Collectively, these data identify the presence of ILCs in the lung of both humans and mice and demonstrate a crucial role for murine lung ILCs in regulating airway epithelial integrity and orchestrating pulmonary tissue homeostasis following experimental influenza virus infection.

Results

Lung-resident ILCs resemble natural helper cells

To examine whether ILCs are present at extra-intestinal mucosal sites, we performed flow cytometric analysis of cells isolated from the lung tissues of naive wild-type C57BL/6 or *Rag1*$^{-/-}$ mice. We identified a population of lineage negative (Lin^{-}) cells that lacked expression of lineage markers associated with T cells (CD3, CD5, TCRβ, CD27), B cells (B220), macrophages (CD11b), dendritic cells (CD11c) or NK cells (NK1.1). These Lin^{-} cells expressed CD90 (Thy1), CD25 (IL-2Rα) and CD127 (IL-7Rα) (Fig. 1a), a pattern of surface marker expression consistent with ILCs[4,5]. Further examination of these Lin^{-} CD90^{+} CD25^{+} lung ILCs revealed a lack of expression of either CD4 or NKp46 (Fig. 1b), thus distinguishing lung-resident ILCs from conventional CD4^{+} LTi cells or NKp46^{+} ILCs[4]. However, lung ILCs did express the activation markers CD44 and ICOS as well as Sca-1 and c-kit (Fig. 1b), similar to the phenotype of nuocytes and NHCs[12,13]. Furthermore, CD90^{+} CD25^{+} lung ILCs expressed the IL-33R subunit T1-ST2 (Fig. 1b). This Lin^{-} population of ILCs was a relatively rare population, totaling 2–3 ×10^{4} cells in naïve mice, representing 0.4–1% of total live cells in the lung (Fig. 1c). Collectively, these data indicate that lung-resident ILCs most closely resemble nuocytes and NHCs, which were originally reported to be present in secondary lymphoid tissue and fat-associated lymphoid clusters (FALCs)[12,13].

Recent studies demonstrated that nuocytes and NHCs can be activated by IL-33 alone or in combination with IL-7 to produce IL-5 and IL-13 (refs. [12,13]). While stimulation of sort-purified CD90^{+} CD25^{+} T1-ST2^{+} lung ILCs with IL-2 and IL-7 had no apparent effect on IL-5 or IL-13 cytokine secretion, the addition of IL-33 resulted in elevated production of both IL-5 and IL-13 (Fig. 1d,e). Unlike CD4^{+} splenic LTi cells (Fig. 1f) or NKp46^{+} ILCs[7–9], CD90^{+} CD25^{+} lung ILCs expressed minimal IL-22 or IL-17A in response to IL-23 stimulation (Fig. 1f,g). Consistent with *in vitro* IL-33 stimulation, administration of recombinant (r)IL-33 *in vivo* resulted in an elevated frequency of lung-resident ILCs that produced the T$_{H}$2 cell-associated cytokines IL-5 and IL-13, but not the T$_{H}$1 cell-associated cytokine interferon-γ (IFN-γ) (Fig. 1h). Taken together, these results indicate that ILCs in

the respiratory tract share a cell surface phenotype and cytokine profile that most closely resembles nuocytes and NHCs.

Lung ILC development requires Id2 but not commensals

Members of the ILC family including LTi cells, NKp46$^+$ ILCs and NHCs share a developmental requirement for the transcriptional regulator Id2 (refs. [12,18–20]). To examine the influence of Id2 on the development of lung-resident ILCs, expression of Id2 was examined in sort-purified lung CD90$^+$ CD25$^+$ ILCs. Quantitative analysis of Id2 mRNA expression revealed comparable abundance of Id2 mRNA in lung-resident ILCs and conventional splenic CD4$^+$ LTi cells (Fig. 2a), a population known to be Id2-dependent[18–20]. Consistent with a developmental requirement for Id2, lung resident CD90$^+$ CD25$^+$ ILCs were not detectable in chimeric mice deficient in Id2 (fig. 2b), thereby developmentally linking this cell population to the Id2-dependent ILC family.

Based on their expression of the transcription factor RORγt, ILCs can be divided into two populations, one of which is critically dependent on RORγt for development (LTi cells, NKp46$^+$ ILCs) and the other group which is RORγt-independent (nuocytes, NHCs)[4]. Compared to splenic LTi cells, lung ILCs did not express abundant RORγt (*Rorc*) mRNA (Fig. 2c) or protein (Fig. 2d), providing further evidence that lung ILCs are more closely related to nuocytes and NHCs than LTi or NKp46$^+$ ILC populations.

Signals derived from commensal bacterial communities have also been implicated in the development and/or activation of several ILC subsets[9,21,22]. To test whether live commensal bacterial-derived signals influenced the development of lung-resident ILCs, we examined ILCs in the lungs of conventional (CNV) or germ-free (GF) C57BL/6 mice. CNV and GF mice had similar frequencies, total numbers, and surface phenotype of lung ILCs (Fig. 2e,f), indicating that development of lung ILCs is dependent on Id2 but independent of signals derived from live commensal bacteria.

ILCs are present in human lung and airways

Recent studies have described heterogeneous populations of LTi-like cells and NKp46$^+$ cells that express IL-17A and/or IL-22 located in human lymphoid tonsil and Peyer's patch tissues[23–27]. However, whether human ILC populations exist at other barrier surfaces such as the respiratory tract and what surface markers they express has not been examined. Similar to findings in mice, we identified a Lin$^-$ population of cells in healthy human lung parenchymal tissue that lacked expression of markers for T cells (CD3, TCRαβ), dendritic cells (CD11c), NK cells (CD56), macrophages (CD11b) or B cells (CD19), but that expressed CD127 (IL-7Rα) (Fig. 3a). The Lin$^-$ CD127$^+$ ILC population in the lung parenchyma expressed CD25 (IL-2Rα) and the IL-33R subunit ST2 (Fig. 3b), consistent with the cell surface phenotype of the lung-resident ILC population found in mouse lung (Fig. 1a,b) and previously identified murine nuocytes and NHCs[12,13]. To determine if an analogous ILC population exists in the airway, we examined bronchoalveolar lavage (BAL) fluid from lung transplant recipients. Similar to the population of ILCs found in lung parenchyma, we identified a Lin$^-$ CD127$^+$ ILC population that also expressed CD25 and ST2 in BAL fluid from 7 of 9 lung transplant recipients examined (Fig. 3c,d). Thus, these

data provide evidence of NHC- and nuocyte-like ILC populations in human respiratory tissue.

Influenza virus induces ILC responses in the lung

ILCs have been shown to mediate anti-bacterial or anti-helminth immunity in the intestine[7,9,11–14]; however, the functional significance of ILCs in regulating immunity and/or inflammation in the lung is not well understood. To investigate whether lung ILCs can influence immunity, inflammation or tissue homeostasis in the lung, we utilized a model of respiratory infection with mouse-adapted H1N1 influenza virus A/Puerto Rico/8/34 (PR8). In response to intranasal PR8 infection, $CD90^+$ $CD25^+$ ILCs accumulated in the lung parenchyma in both wild-type C57BL/6 and *Rag1*$^{-/-}$ mice (Fig. 4a,b). Wild-type mice control viral replication and recover following infection with this dose of PR8 (0.5 LD_{50} or ~300 $TCID_{50}$) and although *Rag1*$^{-/-}$ mice are unable to clear infection and eventually succumb within 12–14 days, the early ILC response and pathologic consequences of infection, including the decline in lung function and lung immunopathology, were similar in immunocompetent and immunodeficient hosts (Supplementary Fig. 1). Taken together, these data demonstrate that ILCs respond to influenza virus infection in the lung in the presence or absence of the adaptive immune system, suggesting a potential role for lung ILCs in regulating innate immunity, inflammation and/or tissue homeostasis in the lung.

ILC depletion impairs lung function and tissue repair

While both cellular and humoral arms of the adaptive immune system have been shown to be crucial for immunity to respiratory viruses, the influence of innate cell populations on anti-viral immunity in the lung remains poorly understood[28]. To examine the influence of lung ILCs on innate immunity to influenza virus, isotype or anti-CD90.2 depleting monoclonal antibodies (mAb) were administered *in vivo* to PR8-infected *Rag1*$^{-/-}$ mice. As some NK cells can also express CD90.2 upon activation, an additional group of mice was treated with anti-NK1.1 mAb to allow direct comparison of anti-CD90.2-mediated depletion of ILCs versus anti-NK1.1-mediated depletion of NK cells. Administration of anti-CD90.2 antibody effectively depleted the $CD90^+$ $CD25^+$ population of ILCs in the lung (Fig. 4c). Depletion of $CD90.2^+$ ILCs or $NK1.1^+$ NK cells did not affect viral loads in the lung compared to isotype treated mice (Fig. 4d), suggesting that neither NK cells nor ILCs directly contribute to innate control of viral replication. However, mice that received anti-CD90.2 mAb exhibited a substantially lower mean body temperature at day 10 post infection (p.i.) (Fig. 4e), indicating exaggerated thermo-dysregulation and morbidity in the absence of $CD90.2^+$ ILCs. Additionally, although neutrophil populations were unaffected by anti-NK1.1 or anti-CD90.2 treatment, eosinophilia was reduced in the BAL fluid of anti-CD90.2-treated mice, likely as a result of reduced IL-5 concentrations in the absence of ILCs (Supplementary fig. 2a,b).

Strikingly, depletion of $CD90.2^+$ ILCs resulted in significantly decreased lung function as measured by pulse oximetry (Pulse Ox), reaching average blood oxygen saturation levels below 54% in anti-CD90.2 treated mice at day 9 p.i. compared to 76% in isotype-treated controls (Fig. 4f). Furthermore, depletion of $CD90.2^+$ ILCs significantly impaired epithelial integrity, as measured by increased total protein concentration in the BAL fluid compared to

isotype or anti-NK1.1 treated mice (Fig. 4g). Influenza is a cytopathic virus that replicates preferentially in airway epithelial cells and causes severe acute injury to the respiratory epithelium[28]. Although isotype-treated or NK cell-depleted *Rag1*$^{-/-}$ mice eventually succumb to infection between day 13–14 due to the absence of an adaptive immune response (data not shown), they generated hyperplastic epithelial and goblet cell responses essential for repair of the damaged airway epithelial barrier (Fig. 4h,i). In contrast to isotype or anti-NK1.1 mAb treatment, depletion of CD90.2^{+} ILCs resulted in an impaired ability to generate hyperplastic epithelial cell responses (Fig. 4j) and led to substantial epithelial degeneration and necrosis (black arrows), including in many cases the complete sloughing of the bronchiolar epithelial lining (Fig. 4j,k). This epithelial necrosis was unlikely to be due to anti-CD90.2 mAb treatment affecting the epithelia directly, as bronchioles in anti-CD90.2 mAb-treated naïve mice had normal epithelial cell lining (Fig. 4l) similar to untreated naïve mice (Fig. 4m). Collectively, these observations indicate a critical role for CD90.2^{+} ILCs in promoting airway epithelial integrity and restoring tissue homeostasis in the lung following acute viral infection.

Lung ILCs are sufficient to restore airway integrity

CD90 is expressed on a number of hematopoietic and non-hematopoietic cell lineages[29]. To address the specificity of the anti-CD90.2-mediated depletion of ILCs, we examined CD90 expression on multiple innate immune cell subsets in the lung. Flow cytometric analysis of macrophages, dendritic cells, neutrophils and eosinophils revealed that these cell subsets lacked expression of CD90.2, suggesting that the anti-CD90.2 mAb was unlikely to have a direct effect on these cell populations (Supplementary fig. 3). To directly test whether lung-resident ILCs were the cell population responsible for promoting tissue remodeling following influenza virus infection, we performed adoptive transfer experiments of congenically disparate CD90.1^{+} lung ILCs into PR8-infected, anti-CD90.2-depleted *Rag1*$^{-/-}$ mice. This system allowed for the selective depletion of endogenous CD90.2^{+} ILCs while leaving the transferred population of CD90.1^{+} lung ILCs unaffected. Analysis of lung tissue by flow cytometry at 10 days p.i. indicated that while anti-CD90.2 mAb effectively abolished host CD90.2^{+} ILC responses in treated mice (Fig. 5a), a population of donor CD90.1^{+} ILCs could be detected (Fig. 5b). CD90.2-depleted mice receiving transferred CD90.1^{+} ILCs exhibited higher mean body temperature at day 10 p.i. compared to mice receiving anti-CD90.2 mAb alone, suggesting that adoptively transferred ILCs can ameliorate influenza-virus induced morbidity (Fig. 5c). Additionally, analysis of blood oxygen saturation levels revealed that delivery of CD90.1^{+} lung ILCs effectively restored lung function to levels equivalent to isotype-treated mice (Fig. 5d). Similar to isotype-treated controls (Fig 5e), anti-CD90.2 treated mice receiving CD90.1^{+} ILCs exhibited regions of epithelial proliferation within the bronchioles (Fig. 5g, black arrows) indicative of a beneficial tissue remodeling response, which was largely absent in mice receiving anti-CD90.2 treatment alone (Fig. 5f, gray arrows). Collectively, these data provide evidence that the lung ILC population, not another CD90-expressing cell type, was critical for promoting respiratory tissue remodeling following influenza virus infection.

IL-33-IL-33R signaling is critical for lung ILC responses

Given the ability of lung ILCs to respond to IL-33 stimulation (Fig. 1e,h) and previous studies demonstrating that IL-33 is upregulated in the lung during influenza virus infection[15,30], we sought to test whether IL-33–IL-33R signaling was required for ILC-dependent maintenance of airway epithelial integrity. Anti-IL-33R (anti-T1-ST2) mAb or PBS was administered to wild-type mice following influenza virus infection. Blockade of IL-33–IL-33R signaling resulted in a significant decrease in both frequency and total cell number of $CD90^+$ $CD25^+$ ILCs in the lungs of anti-IL-33R treated mice compared to PBS treated controls (Fig. 5h-j). Additionally, lung function was severely impaired, with blood oxygen saturation levels reaching 68% in anti-IL-33R treated mice compared to 79% in PBS treated controls (Fig. 5k). Histological examination of lung parenchyma revealed regions of epithelial cell necrosis and bronchial degeneration within the airways of anti-IL-33R treated mice at day 10 p.i. (Fig. 5l,m), indicative of severe damage to the airway epithelial barrier similar to the results observed when ILCs were depleted with anti-CD90.2 mAb (fig. 4j). Taken together, these results confirm the ILC depletion studies and further demonstrate that a treatment that severely impairs lung ILCs can compromise tissue repair and lung function in wild-type mice.

ILC-mediated repair is independent of IL-13 and IL-22

Previous studies demonstrated that IL-13 can promote epithelial cell and goblet cell proliferation as well as epithelial mucin production in the context of airway inflammation and fibrosis[16,31,32]. To test the hypothesis that ILC-derived IL-13 may be required to promote tissue homeostasis following influenza virus infection, rIL-13 was administered to anti-CD90.2-treated *Rag1*$^{-/-}$ mice. Although IL-13 protein could be detected in BAL fluid (Supplementary Fig. 4a) and goblet cell hyperplasia was observed in the bronchioles of rIL-13-treated animals confirming biological activity of the rIL-13 cytokine in the lung (Supplementary Fig. 4b, black arrows), anti-CD90.2-depleted mice receiving rIL-13 had severely decreased blood oxygen saturation levels similar to mice receiving anti-CD90.2 mAb alone (59% compared to 62%, respectively) (Supplementary Fig. 4c). Furthermore, mice receiving anti-CD90.2 alone or in combination with rIL-13 suffered severe influenza-induced morbidity, succumbing to infection four days earlier than isotype-treated mice (day 9 vs. day 13 p.i.) (data not shown). Taken together, these results indicate that rIL-13 is not sufficient to restore lung function in ILC-depleted mice, suggesting that ILCs may employ IL-13-independent mechanisms to promote lung tissue homeostasis.

Intestinal ILCs express IL-22 and that IL-22–IL-22R interactions regulate intestinal immunity[7,9,26]. To test whether IL-22 influenced airway epithelial barrier function following exposure to influenza virus, infected wild-type mice were treated with isotype control or anti-IL-22 neutralizing mAb. Neutralization of IL-22 in infected mice resulted in similar rates of weight loss and decline in blood oxygen saturation levels compared to control mice (Supplementary Fig. 5a,b) and examination of lung pathology showed no apparent defect in the ability of infected mice to mount a hyperproliferative epithelial remodeling response (Supplementary Fig. 5c). Consistent with a recent report[33], these data indicate that blockade of IL-22–IL-22R signaling does not substantially influence restoration of lung tissue homeostasis following influenza virus infection.

Wound healing genes are enriched in ILCs

To investigate potential mechanisms by which lung ILCs influence maintenance of airway epithelial integrity or restoration of lung tissue homeostasis, we performed genome-wide transcriptional profiling of lung-resident ILCs. $CD90^+$ $CD25^+$ lung ILCs and $CD90^+$ $CD4^+$ spleen LTi cells were sort-purified from the lungs or spleens of naïve C57BL/6 mice and mRNA isolated from these populations was then hybridized to Affymetrix GeneChips for genome-wide transcriptional profiling. Examination of the top 100 genes differentially expressed in lung ILCs compared to splenic LTi cells illustrated substantial differences between these two ILC populations (Fig. 6a). Splenic LTi cells were characterized by high expression of CD4, CCR6, IL-23R and RORγt, in agreement with previous studies[7,8], while the top transcripts in the lung ILCs included the ST2 receptor IL1Rl1, IL-25 receptor IL-17Rb, and the cytokines IL-2 and IL-5 (Fig. 6b). In addition, within the top 100 genes expressed in lung ILCs, there was striking expression of multiple genes associated with tissue remodeling, including genes encoding the extracellular matrix proteins decorin, asporin and dermatopontin as well as epidermal growth factor family members like amphiregulin (Fig. 6b). Analysis of the differentially expressed genes between lung ILC versus splenic LTi cell populations using the Database for Annotation, Visualization and Integrated Discovery (DAVID) revealed a transcriptional signature of lung ILCs that was significantly enriched in pathways regulating wound healing, immune defense responses, inflammatory responses and cell proliferation (Fig. 6c and Supplementary Table 1). In contrast, splenic LTi cells were significantly enriched in processes associated with hematopoietic and lymphoid organ development, immune responses, and cell activation (Fig. 6c and Supplementary Table 1).

Gene Set Enrichment Analysis (GSEA) was then employed to compare the gene expression signature of lung ILCs with previously reported models of lung damage or inflammation. Direct comparison of the lung ILC gene set with a previously published data set examining the effects of lipopolysaccharide (LPS)-induced acute lung injury[34] revealed enrichment of the transcriptional signatures of lung ILCs in the LPS-treated group compared to PBS-treated controls, consistent with a signature of tissue damage and wound repair (Fig. 6d). Further analysis of the transcripts which most contributed to the bias toward the LPS-treated group (denoted by the ‘leading edge’) revealed the presence of the gene amphiregulin (*Areg*). Thus, this epidermal growth factor, which was highly expressed in the lung ILC gene expression profile, is one of the strong “driver genes” in this enrichment pattern (Fig. 6d and Supplementary Table 2). Collectively, these results represent the first genome-wide transcriptional profiling of lung ILCs and demonstrate clear gene signatures of wound healing in the lung ILC population.

Amphiregulin restores lung function in ILC-depleted mice

Amphiregulin is a member of the EGF family of growth factors that has been implicated in regulating tissue remodeling and repair in the context of acute epithelial injury and asthma[35–37]. Quantitative qPCR analysis confirmed the microarray results demonstrating high expression of amphiregulin mRNA by lung ILCs compared to splenic LTi cells (Fig. 7a). Further, stimulation of sort-purified $CD90^+$ $CD25^+$ T1-$ST2^+$ lung ILCs with IL-2 and IL-7 in combination with IL-33 resulted in elevated production of amphiregulin protein

compared to culture with IL-2 and IL-7 alone (Fig. 7b). Analysis of lung parenchyma tissue in *Rag1*$^{-/-}$ mice at 10 days post-influenza virus infection revealed a significant increase in amphiregulin mRNA (Fig. 7c) and protein expression (Fig. 7d) compared to naïve controls, indicating that amphiregulin expression is upregulated in the lung following influenza virus infection and airway damage. Analysis of lung tissue from anti-CD90.2 treated mice revealed reduced amphiregulin mRNA in the absence of CD90.2^{+} ILCs (Fig. 7e), indicating that lung ILCs are a major source of amphiregulin *in vivo* and that secretion of this protein may be one mechanism by which ILCs promote airway epithelial integrity and restore lung function.

To directly test whether delivery of amphiregulin could promote airway epithelial integrity and restore lung function following influenza virus-induced damage, recombinant amphiregulin was administered to anti-CD90.2 treated PR8-infected *Rag1*$^{-/-}$ mice (Fig. 7f). While IL-5 and IL-13 expression levels in the lung were not significantly altered following amphiregulin treatment (Supplementary Fig. 6a,b), mice receiving recombinant amphiregulin exhibited substantially higher mean body temperatures (Fig. 7g) and significantly improved lung function compared to anti-CD90.2 treated controls, reaching blood oxygen saturation levels comparable to isotype-treated mice at day 9 p.i. (78% vs 80%, respectively) (Fig. 7h). Additionally, mice treated with recombinant amphiregulin exhibited diminished amounts of total protein present in the BAL fluid compared to anti-CD90.2-treated controls (Fig. 7i) and histologic analysis of lungs from anti-CD90.2-depleted mice receiving recombinant amphiregulin revealed regions of epithelial cell hyperplasia and goblet cell proliferation (black arrows) within the bronchial airways indicating that recombinant amphiregulin treatment promoted restoration of airway epithelial integrity and lung tissue homeostasis (Fig. 7j-l). Collectively, these data provide both *in vitro* and *in vivo* evidence implicating amphiregulin as one mechanism by which ILCs can promote tissue homeostasis following influenza virus infection.

Discussion

A number of studies have identified heterogeneous ILC populations in the murine and human intestine and implicated a role for these cell populations in regulating immunity and inflammation in the gut[4,5]. The data presented in this report identify a population of ILCs constitutively present in the respiratory tract of humans and mice and demonstrate a novel function for murine lung ILCs in regulating airway epithelial barrier integrity and tissue homeostasis following influenza virus-induced pulmonary damage.

The ILC population in mice is remarkably heterogeneous and includes cell populations found in lymphoid and intestinal tissues that exhibit distinct developmental requirements and patterns of effector cytokine expression[4,5]. In this report, we show that the development of lung-resident ILCs in mice is Id2-dependent and that these cells express a panel of cell surface markers characteristic of other ILC populations, including CD90, CD25, CD127 and T1-ST2. Furthermore, lung-resident ILCs produced IL-5 and IL-13 in response to IL-33 stimulation, but notably did not make high amounts of IL-22 or IL-17A following culture with IL-23. The cell surface phenotype and cytokine profile of these lung-resident ILCs indicate that they most closely resemble NHCs or nuocytes, cell types previously thought to

be restricted to sites within the gut-associated lymphoid tissue and fat-associated lymphoid clusters[4,5,12,13]. It remains to be determined whether ILCs in the murine respiratory tract constitute a defined subset of ILCs distinct from nuocytes or NHCs, or whether these ILC populations are developmentally related cells existing in multiple anatomical locations.

In humans, previous studies identified RORγt^+ ILC populations in the tonsils and Peyer's patches that share a phenotype and cytokine profile similar to mouse LTi cells and NKp46$^+$ ILCs[23–27]. In this report, we provide the first identification of ILCs in the human respiratory tract and lung parenchyma. Human lung ILCs expressed CD25, CD127 and ST2 (IL-33R), indicating they are a nuocyte/NHC-like ILC. Therefore, like murine ILCs, human ILC populations exhibit heterogeneity in tissue distribution, phenotype and functional capacity. Examining other lymphoid and mucosal-associated tissues may lead to the identification of additional ILC-like cells and provide insight into the regulation of human ILC populations.

While previous studies have implicated NHCs and nuocytes in promoting T_H2 cytokine-dependent anti-helminth immunity[4,5,12,13], we identify a role for ILCs in repairing airway epithelial integrity and maintaining lung tissue homeostasis. Lung injury is a key feature of many diseases including viral infections such as influenza virus, but also COPD, ARDS, Sarcoidosis, asthma, allergy and others[16,17]. However, the mechanisms involved in effective versus ineffective lung repair and tissue remodeling are poorly understood. The identification of lung ILCs as an important cell type regulating tissue homeostasis not only implicates a new hematopoietic cell type in orchestration of non-hematopoietic cell repair/regeneration, but also reveals previously unappreciated functions for the ILC lineage.

Genome-wide transcriptional profiling revealed expression of a number of genes associated with wound healing and tissue repair by lung ILC including extracellular matrix proteins decorin, asporin and dermatopontin as well as epidermal growth factor family members like amphiregulin. Amphiregulin is expressed in multiple organs including the lung and has been shown to play critical roles in wound repair and tissue remodeling through promotion of epithelial cell and fibroblast proliferation in settings of cancer, acute epithelial injury and asthma[35,36,38,39]. The demonstration that lung ILCs express high levels of amphiregulin, that depletion of ILCs results in loss of amphiregulin expression and that administration of amphiregulin to ILC-depleted mice following influenza virus infection can restore epithelial integrity and tissue repair, indicates that ILC-derived amphiregulin is one mechanism through which ILCs regulate lung homeostasis.

The T_H2 cell cytokines IL-5 and IL-13 have also been shown to mediate epithelial cell and goblet cell hyperplasia in the lung[31,32,40]. Although lung-resident ILCs were capable of producing high amounts of IL-5 and IL-13 in response to IL-33 stimulation, the administration of IL-13 failed to restore lung function or promote respiratory tissue remodeling in influenza virus-infected ILC-depleted mice, thus distinguishing the tissue repair functions of lung ILCs from other nuocyte and NHC populations that are reported to act primarily through IL-13-dependent mechanisms[12–15]. It is currently unclear whether this difference indicates a minor role for IL-13 in the disease context examined here or additional heterogeneity in the functional diversity of ILC populations in the lungs. It is important to note that ILC-derived IL-13 might play a more prominent role in other airway

disease contexts. For example, a recent report found a role for NHC-derived IL-13 using a different H3N1 influenza virus infection model that causes airway hyperreactivity early during infection[15]. In those studies, however, the NHC-produced IL-13 contributed to airway hyperreactivity suggesting that in some settings the type 2 cytokines produced by lung ILC populations might have detrimental effects.

The impact of lung ILC-derived cytokines and tissue remodeling proteins might depend on the pattern of lung injury (i.e. different pathogenesis of infectious or inflammatory disease) or other environmental factors. Nonetheless, the identification of a major pathway of tissue repair coordinated by lung ILCs suggests that these cells, and their products, could be targets for therapeutic manipulation in settings of lung infection, injury and chronic inflammation. Future studies are needed to fully characterize the different subtypes of ILCs that might exist in the respiratory tract. Comparison of the transcriptional profiles of the diverse ILC populations such as those presented here will be an important tool for elucidating the lineage relationships between RORγt-dependent LTi cells and RORγt-independent ILCs as well as highlighting biological features unique to these different cell types. In the context of lung inflammation and damage, it will be important to determine the extent of potential crosstalk between the epithelial repair pathways induced by IL-13 and the tissue repair/remodeling proteins such as amphiregulin expressed by lung ILC. It is interesting to note that IL-33, as a key product made by epithelial and immune cell lineages, can induce both IL-13 and amphiregulin production by lung ILCs, indicating that a degree of crosstalk exists between the damaged tissue and the ILC population that initiates the repair process.

In summary, the results presented in this report identify a previously unrecognized role for lung ILCs in promoting airway epithelial integrity and lung tissue homeostasis through production of the epidermal growth factor family member amphiregulin. In light of these new findings, targeting ILC responses in the airway and other tissues may offer new therapeutic potential in the clinical management of tissue damage or chronic inflammation.

Methods

Mice

C57BL/6 wild-type (WT) mice and *Rag1*$^{-/-}$ were purchased from the Jackson Laboratory. All mice were maintained in specific pathogen-free facilities at the University of Pennsylvania. All protocols were approved by the University of Pennsylvania Institutional Animal Care and Use Committee (IACUC), and all experiments were performed according to the guidelines of the University of Pennsylvania IACUC. Germ-free mice were maintained in plastic isolator units, fed autoclaved feed and water, and routinely monitored to ensure absence of microbial contamination. Generation of Id2-deficient mice and fetal liver chimeras have been described previously[41,42]. For generation of Id2-deficient bone marrow chimeras, 10–20 × 10^6 bone marrow cells from *Id2*$^{+/+}$ or *Id2*$^{-/-}$ fetal liver chimeras were transferred i.v. into irradiated hosts (900 RAD) of a different congenic marker. All chimeras were placed on antibiotic drinking water (Sulfamethoxazole and Trimethoprim, Hi-Tech Pharmacal Co.) for two weeks following irradiation and were allowed to reconstitute for 10 weeks prior to analysis.

Flow cytometry

Single cell suspensions were stained with a combination of the following monoclonal fluorescently conjugated antibodies: FITC-conjugated T1/ST2 (DJ8; MD Bioproducts). PE-conjugated ICOS (7E.17G9), Sca-1 (D7), c-kit (2B8), NKp46 (29AI.4), Siglec F (E50-2440; BD Pharmigen). PerCP-Cy5.5-conjugated CD3 (17A2), CD5 (53–73), CD27 (LG.7F9), NK1.1 (PK136), TCRβ H57597, CD11b (MI/70), CD11c (N418), B220 (RA3-6B2). APC-conjugated CD44 (IM7), c-kit (2B8), CD90.1 (HIS51). eFluor-450-conjugated CD127 (A7R34), CD45.1 (A20). PE-Cy7-conjugated CD25 (PC61.5). Alexa 700-conjugated CD90.2 (30-H12) and Ly6G (1A8; Biolegend). e-Fluor-780-conjugated CD11b (MI/70), CD11c (N418), TCRβ (H57-597), B220 (RA3-6B2), CD45.2 (104). PE-Texas Red-conjugated CD4 (GK1.5; Abcam). All antibodies were purchased from eBioscience unless specified otherwise. For measurement of intracellular cytokine expression, stimulated cells were surface stained with a combination of the antibodies listed above, fixed and permeabilized using a commercially available kit (eBioscience), and stained with IL-5 APC (TRFK5; BD Pharmigen), IL-13-PE (eBio13A; eBioscience), IL-17A PE (TC11-18H10; BD Pharmigen), or IL22-02 (from Pfizer Inc.) conjugated to Alexa Fluor 647 according to manufacturer's instructions (Molecular Probes). For measurement of intracellular RORγt, cells were fixed, permeabilized and stained with RORγt PE (AFKJS-9; eBioscience) For all stains, dead cells were excluded from analysis by means of an Aqua viability stain (Invitrogen). Samples were acquired on a BD LSRII flow cytometer (BD Biosciences) and analyzed using FlowJo software (v9.2, Tree Star)

Isolation of cells from mouse lung tissue

Lungs were perfused with 10 ml PBS through the right ventricle of the heart prior to removal. Lungs were then cut into small pieces using scissors and digested with 1 mg/ml Collagenase D (Roche) in PBS for 30–45 min at 37 °C with vortexing every 10 min. Samples were mashed through 70 μm cell strainers, washed with DMEM media (supplemented with 10% FBS, 1% L-glutamine (GIBCO), 1% Pencillin/Streptomycin (GIBCO)), and any remaining red blood cells were lysed. Single cell suspensions were used for subsequent flow cytometry staining.

Analysis of human BAL fluid and lung

Human bronchoalveolar lavage samples were obtained as residual material from clinical procedures from nine patients undergoing routine surveillance bronchoscopies during the first year following lung transplant. Patients were on a regimen of immunomodulatory drugs following lung transplant, including tacrolimus and prednisone in addition to either mycophenolate or azathioprine. Use of human BAL samples for research purposes was approved by the University of Pennsylvania IRB and carried out in accordance with protocols for use of residual clinical material with waiver of consent.

Human lung tissue was obtained from cadaver organ donors in collaboration with the New York Organ donor network (NYODN, New York, NY). Consent was obtained for use of lung tissue from human cadavers for research purposes. Lung tissue was cut into small pieces with a curved scissor and subsequently incubated at 37 °C with shaking for 1 h in collagenase solution (1 mg/ml Collagenase D, 1 mg/ml Trypsin Inhibitor and 25 μg/ml

DNAse I). The tissue was then mechanically dissociated using a gentleMACS Dissociator (Miltenyi Biotech) and strained with a wire mesh tissue sieve. Remaining connective tissue was then removed by passing the cell suspension through a syringe column fitted with glass wool. Lymphocytes were subsequently separated by centrifugation through Ficoll (LSM, Invitrogen).

For analysis of ILC populations, single cell suspensions of BAL fluid and lung parenchyma were stained with the following monoclonal antibodies for flow cytometric analysis: ST2 FITC (B4E6; MD Bioproducts), CD3 PerCP-Cy5.5 (SK7; BD Pharmigen, intracellular staining), CD11b APC (MI/70; eBioscience), CD19 eFluor 450 (HIB19; eBioscience), CD25 PE-Cy7 (M-A251) BD Pharmigen), CD56 Alexa Fluor 700 (CMSSB; BD Pharmigen), CD127 eFluor 780 (eBioRDR5; eBioscience), CD11c PE-Cy5 (B-ly6) BD Pharmigen) and TCRαβ PE-Cy5 (IP26; eBioscience), live/dead aqua stain (Invitrogen). Samples were acquired on a BD LSRII flow cytometer (BD Biosciences) and analyzed using FlowJo software (v9.2, Tree Star).

RNA isolation and Real-Time Quantitative PCR

RNA was isolated from purified populations of $CD90^+$ $CD25^+$ lung ILCs, $CD90^+$ $CD4^+$ splenic LTi cells or $B220^+$ splenic B cells, sorted using a BD FACSAria (BD Biosciences) cell sorter. RNA was isolated using RNeasy mini kit according to manufacturer's instructions (QIAGEN). cDNA was generated using Superscript reverse transcription (Invitrogen). Real-time quantitative PCR (qRT-PCR) was performed on cDNA using SYBR green master mix (Applied Biosystems) and commercially available primer sets (QIAGEN). Reactions were run on a real-time PCR system (ABI7500; Applied Biosystems). Samples were normalized to β-actin and displayed as a fold induction relative to expression seen in purified B cells (*Id2* and *Rorc*) or naïve lung tissue (*Areg*, *Il5* and *Il13*).

Cytokine ELISA

$CD90^+$ $CD25^+$ $T1/ST2^+$ lung ILCs were sort-purified from the lungs of C57BL/6 mice using a BD FACSAria cell sorter. 2×10^4 lung ILCs were cultured in DMEM complete media in the presence of 10 ng/ml rmIL-7, 10 ng/ml rIL-2, and/or 30 ng/ml rmIL-33 (for measurement of IL-5, IL-13 and amphiregulin) or 50 ng/ml rmIL-23 (for measurement of IL-17A) for four days (all recombinant cytokines obtained from R&D Systems). Supernatants were collected after 4 days of culture. For measurement of amphiregulin in whole tissue, lung tissues from naïve or PR8 influenza-infected mice were homogenized in sterile PBS and centrifuged to remove cell debris. Measurement of IL-5, IL-13 and IL-17A were performed using commercially available ELISA kits (eBioscience). Amphiregulin was measured using DuoSet ELISA Kit (R&D Systems).

Influenza infection, antibody treatments and cytokine administration

For infections with PR8 influenza virus, C57BL/6 or *Rag1*$^{-/-}$ mice were anaesthetized with 2.5% Avertin i.p. and infected with 0.5 LD50 PR8-GP33 virus (recombinant virus expressing the LCMV epitope GP33) in 25μl volume administered intransally. PR8-GP33 influenza virus was grown and titered as previously described[43]. The replication and

pathogenicity of this recombinant PR8 strain was not substantially different from nonrecombinant virus[39].

For monoclonal antibody treatments, anti-CD90.2 mAb (30H12) and anti-NK1.1 mAb (PK136) were purchased from BioXCell (West Lebanon, NH). Anti-IL-33R mAb (anti-ST2 clone 245707) was purchased from R&D Systems. Anti-IL-22 mAb (IL-22-01) was provided by Pfizer Inc. All mAb treatments were administered i.p. every 3 days at a dose of 200 μg/mouse starting on the day prior to infection.

For cytokine treatments, recombinant murine IL-13 or amphiregulin (R&D Systems) was administered i.p. every 2 days at a dose of 5–10 μg starting on the day of infection.

ILC adoptive transfer

1×10^5 Lin^- $CD90^+$ $CD25^+$ T1-$ST2^+$ ILCs were sort-purified from the lungs of naïve CD90.1 wild-type mice and transferred intravenously into anti-CD90.2 mAb-treated *Rag1*$^{-/-}$ mice at day 0 and day 5 post influenza virus infection (0.5 LD_{50} PR8).

Lung histological sections

Left lobes of lungs were perfused and fixed with 4% paraformaldehyde, embedded in paraffin, and 5 μm sections were used for staining with H&E.

Measurement of Pulse Oximetry

The MouseOxTM Pulse-oximeter (Starr Life Sciences) was used to measure blood SpO_2 in PR8-infected mice during the course of infection. A depilatory agent (Nair, Church & Dwight Co.) was applied to the neck of anesthetized mice 2 days prior to influenza infection to remove hair and delay future hair growth. For readings, the oximeter clip was placed on the neck and percent SpO_2 was measured each second over several minutes, data shown is average of SpO_2 readings recorded over 3–5 min per mouse.

Measurement of BAL fluid protein concentration

Bronchoalveolar lavage fluid was collected from naïve or PR8-infected mice using the following method. A small cut was made in the trachea and a thin tube was inserted. Lungs were lavaged using 500 μl PBS and fluid was immediately placed on ice. BAL fluid was spun down to pellet cells and cell-free supernatant was collected. Measurement of total protein was performed using a Micro BCA protein assay (Pierce Thermo Scientific) according to manufacturer's instructions.

Influenza virus quantification

Lung tissue was homogenized and RNA was isolated using RNeasy mini kit according to manufacturer's instructions (QIAGEN). cDNA was generated using MultiScribe reverse transcription (Invitrogen). Real-time quantitative PCR (qRT-PCR) was performed on cDNA using FAM/TAM system (Applied Biosystems). Primers and Taqman probe were generated that were specific for M1 protein of PR8-GP33 influenza virus. Reactions were run on a real-time PCR system (ABI7500; Applied Biosystems). Viral RNA concentration (ng per gram of lung tissue) in each sample was determined by comparison to a standard curve of

PR8-GP33 virus RNA concentrations and converted to μl of virus per gram of lung tissue. The TCID50 of PR8-GP33 per μl of virus was determined with a plaque assay on Madin-Darby canine kidney (MDCK) cell monolayers as previously described[39]. The $TCID_{50}$ per μl of virus was then multiplied by the μl of virus present in the lung tissue to determine the $TCID_{50}$ equivalence.

Microarray gene expression profiling

Lin^- $CD90^+$ $CD25^+$ ILCs and Lin^- $CD90^+$ $CD4^+$ LTi cells were sorted from the lungs (ILC) and spleens (LTi cell) of naïve C57BL/6 wild-type mice. Four biological replicates were collected, each consisting of 15,000–20,000 cells sorted from 6 pooled lungs (ILCs) or 10 pooled spleens (LTi cells) to > 97% purity. Cells were sorted directly into TRIzol LS (Invitrogen). mRNA was isolated, amplified, and hybridized to Affymetrix GeneChips (Mouse Gene 1.0ST).

Data Normalization and Differential Gene Expression Profiling

Affymetrix Power Tools software was used to process and quantile normalize fluorescent hybridizaiton signals using the Robust Multichip Averaging (RMA) method[44]. Transcripts were $\log_2$ normalized and technical replicates were averaged for fold-change analysis. Using the ClassNeighbors module of GenePattern, genes were ranked by the signal-to-noise ratio and class-biased genes were identified by permutation testing[45]. Genes were considered differentially expressed if the fold-change was > 2, $P < 0.05$.

GO Enrichment Analysis

Differentially expressed genes (fold-change > 2) in both the naïve ILC and naïve LTi transcriptional profiles were uploaded to the Database for Annotation, Visualization and Integrated Discovery (DAVID, http://david.abcc.ncifcrf.gov/)[46], and Fischer's exact test was used to identify significantly enriched Gene Ontology (GO, http://www.geneontology.org) terms[46]. (Full list of enriched genes for specific GO terms listed in Fig. 6c available in Supplementary Table 1).

Gene Set Enrichment Analysis (GSEA)

Gene Set Enrichment Analysis (GSEA) was performed using the Broad Institute program (http://www.broadinstitute.org/gea/index.jsp) as described previously[47]. Published gene expression arrays of whole lungs divided into either "control" or "LPS-treated" groups were downloaded from Gene Expression Omnibus (GEO, www.ncbi.nlm.nih.gov/geo/)[34]. The normalized enrichment score (NES) and q-value were calculated for enrichment of the top 100 differentially expressed genes from the ILC naïve data sets (as previously defined using the ClassNeighbors signal-to-noise ratio) between the publically accessible gene arrays (described above). (Leading-edge genes listed in Supplementary Table 2.)

Statistical analysis

Results represent the mean ± SEM unless indicated otherwise. Statistical significance was determined by unpaired Student's *t* test. Statistical analyses were performed using Prism GraphPad software v5.0. (*,$P < 0.05$; **, $P < 0.01$; ***, $P < 0.001$).

Supplementary Material

Refer to Web version on PubMed Central for supplementary material.

Acknowledgements

We would like to acknowledge all members of the Artis lab and Wherry lab, and in particular M. Siracusa, S. Saenz, L. Osborne, E. Tait Wojno, M. Noti, M. Nair and A. Crawford for helpful discussions and critical reading of the manuscript. We thank D. Kobuley and D. Hill for care of the germ-free mouse facility. We thank A. Yadav and A. Fitzgerald for assistance with the human BAL samples. We also thank L. Fouser, S. Olland, R. Zollner, K. Lam and A. Root at Pfizer Inc. for the preparation of IL-22 antibodies. Research in the Wherry lab is supported by National Institute of Health (U19AI083022, AI071309, and HHSN266200500030C) to E.J.W. Human pulmonary BAL studies are supported by National Institute of Health HL098957 to R.G.C. Research in the Artis lab is supported by National Institute of Health (AI061570, AI074878, AI087990, AI095608, AI091759, AI095466, U01AI095608 to D.A).; L.A.M and G.F.S. are funded by T32AI007532-08; M.C.A is funded by T32AI05528; the Burroughs Wellcome Fund (Investigator in Pathogenesis of Infectious Disease Award to D.A.), and pilot grants from the University of Pennsylvania (VCID, PGFI and University Research Fund to D.A).

References

1. Turner JR. Intestinal mucosal barrier function in health and disease. Nat Rev Immunol. 2009; 9:799–809. [PubMed: 19855405]
2. Artis D. Epithelial-cell recognition of commensal bacteria and maintenance of immune homeostasis in the gut. Nat Rev Immunol. 2008; 8:411–420. [PubMed: 18469830]
3. Sonnenberg GF, Fouser LA, Artis D. Functional biology of the IL-22-IL-22R pathway in regulating immunity and inflammation at barrier surfaces. Adv Immunol. 2010; 107:1–29. [PubMed: 21034969]
4. Spits H, Di Santo JP. The expanding family of innate lymphoid cells: regulators and effectors of immunity and tissue remodeling. Nat Immunol. 2011; 12:21–27. [PubMed: 21113163]
5. Saenz SA, Noti M, Artis D. Innate immune cell populations function as initiators and effectors in Th2 cytokine responses. Trends Immunol. 2010; 31:407–413. [PubMed: 20951092]
6. Rankin L, Belz GT. Diverse roles of inhibitor of differentiation 2 in adaptive immunity. Clin Dev Immunol 2011. 2011
7. Sonnenberg GF, Monticelli LA, Elloso MM, Fouser LA, Artis D. CD4(+) lymphoid tissue-inducer cells promote innate immunity in the gut. Immunity. 2011; 34:122–134. [PubMed: 21194981]
8. Takatori H, et al. Lymphoid tissue inducer-like cells are an innate source of IL-17 and IL-22. J Exp Med. 2009; 206:35–41. [PubMed: 19114665]
9. Satoh-Takayama N, et al. Microbial flora drives interleukin 22 production in intestinal NKp46+ cells that provide innate mucosal immune defense. Immunity. 2008; 29:958–970. [PubMed: 19084435]
10. Buonocore S, et al. Innate lymphoid cells drive interleukin-23-dependent innate intestinal pathology. Nature. 2010; 464:1371–1375. [PubMed: 20393462]
11. Saenz SA, et al. IL25 elicits a multipotent progenitor cell population that promotes T(H)2 cytokine responses. Nature. 2010; 464:1362–1366. [PubMed: 20200520]
12. Moro K, et al. Innate production of T(H)2 cytokines by adipose tissue-associated c-Kit(+)Sca-1(+) lymphoid cells. Nature. 2010; 463:540–544. [PubMed: 20023630]
13. Neill DR, et al. Nuocytes represent a new innate effector leukocyte that mediates type-2 immunity. Nature. 2010; 464:1367–1370. [PubMed: 20200518]
14. Price AE, et al. Systemically dispersed innate IL-13-expressing cells in type 2 immunity. Proc Natl Acad Sci U S A. 2010; 107:11489–11494. [PubMed: 20534524]
15. Chang YJ, et al. Innate lymphoid cells mediate influenza-induced airway hyper-reactivity independently of adaptive immunity. Nat Immunol. 2011; 12:631–638. [PubMed: 21623379]
16. Crosby LM, Waters CM. Epithelial repair mechanisms in the lung. Am J Physiol Lung Cell Mol Physiol. 2010; 298:L715–L731. [PubMed: 20363851]

17. Rock JR, Hogan BL. Epithelial Progenitor Cells in Lung Development, Maintenance, Repair, and Disease. Annu Rev Cell Dev Biol. 2011
18. Yokota Y, et al. Development of peripheral lymphoid organs and natural killer cells depends on the helix-loop-helix inhibitor Id2. Nature. 1999; 397:702–706. [PubMed: 10067894]
19. Satoh-Takayama N, et al. IL-7 and IL-15 independently program the differentiation of intestinal CD3-NKp46+ cell subsets from Id2-dependent precursors. J Exp Med. 2010; 207:273–280. [PubMed: 20142427]
20. Boos MD, Yokota Y, Eberl G, Kee BL. Mature natural killer cell and lymphoid tissue-inducing cell development requires Id2-mediated suppression of E protein activity. J Exp Med. 2007; 204:1119–1130. [PubMed: 17452521]
21. Sanos SL, et al. RORgammat and commensal microflora are required for the differentiation of mucosal interleukin 22-producing NKp46+ cells. Nat Immunol. 2009; 10:83–91. [PubMed: 19029903]
22. Sawa S, et al. RORgammat(+) innate lymphoid cells regulate intestinal homeostasis by integrating negative signals from the symbiotic microbiota. Nat Immunol. 2011; 12:320–326. [PubMed: 21336274]
23. Crellin NK, et al. Regulation of cytokine secretion in human CD127(+) LTi-like innate lymphoid cells by Toll-like receptor 2. Immunity. 2010; 33:752–764. [PubMed: 21055975]
24. Cupedo T, et al. Human fetal lymphoid tissue-inducer cells are interleukin 17-producing precursors to RORC+ CD127+ natural killer-like cells. Nat Immunol. 2009; 10:66–74. [PubMed: 19029905]
25. Hughes T, et al. Interleukin-1beta selectively expands and sustains interleukin-22+ immature human natural killer cells in secondary lymphoid tissue. Immunity. 2010; 32:803–814. [PubMed: 20620944]
26. Cella M, et al. A human natural killer cell subset provides an innate source of IL-22 for mucosal immunity. Nature. 2009; 457:722–725. [PubMed: 18978771]
27. Cella M, Otero K, Colonna M. Expansion of human NK-22 cells with IL-7, IL-2, and IL-1beta reveals intrinsic functional plasticity. Proc Natl Acad Sci U S A. 2010; 107:10961–10966. [PubMed: 20534450]
28. Kohlmeier JE, Woodland DL. Immunity to respiratory viruses. Annu Rev Immunol. 2009; 27:61–82. [PubMed: 18954284]
29. Bradley JE, Ramirez G, Hagood JS. Roles and regulation of Thy-1, a context-dependent modulator of cell phenotype. Biofactors. 2009; 35:258–265. [PubMed: 19422052]
30. Le Goffic R, et al. Influenza Virus Infection Induces IL-33 in Mouse Lungs. Am J Respir Cell Mol Biol. 2011
31. Doherty T, Broide D. Cytokines and growth factors in airway remodeling in asthma. Curr Opin Immunol. 2007; 19:676–680. [PubMed: 17720466]
32. Wilson MS, Wynn TA. Pulmonary fibrosis: pathogenesis, etiology and regulation. Mucosal Immunol. 2009; 2:103–121. [PubMed: 19129758]
33. Guo H, Topham DJ. Interleukin-22 (IL-22) production by pulmonary Natural Killer cells and the potential role of IL-22 during primary influenza virus infection. J Virol. 2010; 84:7750–7759. [PubMed: 20504940]
34. Altemeier WA, et al. Modulation of lipopolysaccharide-induced gene transcription and promotion of lung injury by mechanical ventilation. J Immunol. 2005; 175:3369–3376. [PubMed: 16116230]
35. Enomoto Y, et al. Tissue remodeling induced by hypersecreted epidermal growth factor and amphiregulin in the airway after an acute asthma attack. J Allergy Clin Immunol. 2009; 124:913–920. e911–e917. [PubMed: 19895983]
36. Fukumoto J, et al. Amphiregulin attenuates bleomycin-induced pneumopathy in mice. Am J Physiol Lung Cell Mol Physiol. 2010; 298:L131–L138. [PubMed: 19915156]
37. Dolinay T, et al. Gene expression profiling of target genes in ventilator-induced lung injury. Physiol Genomics. 2006; 26:68–75. [PubMed: 16569776]
38. Wang SW, et al. Amphiregulin expression in human mast cells and its effect on the primary human lung fibroblasts. J Allergy Clin Immunol. 2005; 115:287–294. [PubMed: 15696083]

39. Okumura S, Sagara H, Fukuda T, Saito H, Okayama Y. FcepsilonRI-mediated amphiregulin production by human mast cells increases mucin gene expression in epithelial cells. J Allergy Clin Immunol. 2005; 115:272–279. [PubMed: 15696081]

40. Broide DH. Immunologic and inflammatory mechanisms that drive asthma progression to remodeling. J Allergy Clin Immunol. 2008; 121:560–570. [PubMed: 18328887]

41. Cannarile MA, et al. Transcriptional regulator Id2 mediates CD8+ T cell immunity. Nat Immunol. 2006; 7:1317–1325. [PubMed: 17086188]

42. Monticelli LA, et al. Transcriptional regulator Id2 controls survival of hepatic NKT cells. Proc Natl Acad Sci U S A. 2009; 106:19461–19466. [PubMed: 19884494]

43. Decman V, et al. Cell-intrinsic defects in the proliferative response of antiviral memory CD8 T cells in aged mice upon secondary infection. J Immunol. 2010; 184:5151–5159. [PubMed: 20368274]

44. Irizarry RA, et al. Exploration, normalization, and summaries of high density oligonucleotide array probe level data. Biostatistics. 2003; 4:249–264. [PubMed: 12925520]

45. Reich M, et al. GenePattern 2.0. Nat Genet. 2006; 38:500–501. [PubMed: 16642009]

46. Huang da W, et al. Extracting biological meaning from large gene lists with DAVID. Curr Protoc Bioinformatics. 2009 Chapter 13, Unit 13 11.

47. Subramanian A, et al. Gene set enrichment analysis: a knowledge-based approach for interpreting genome-wide expression profiles. Proc Natl Acad Sci U S A. 2005; 102:15545–15550. [PubMed: 16199517]

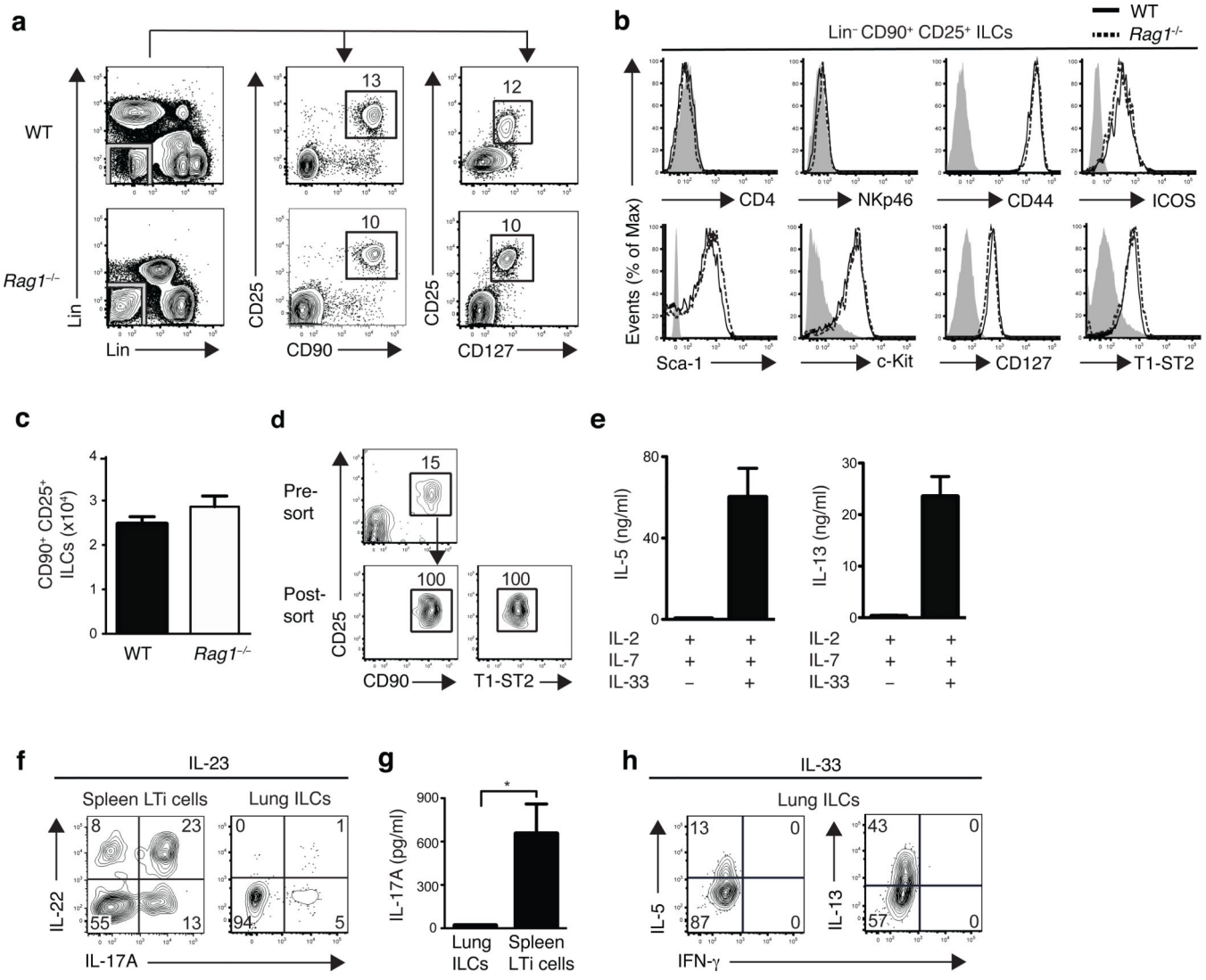

Figure 1. ILCs in the lung resemble nuocytes and NHCs in phenotype and cytokine profile

(**a**) Identification of lung ILCs in C57BL/6 wild-type (WT) and *Rag1*$^{-/-}$ mice by flow cytometry as CD90^{+} CD25^{+} CD127^{+} lineage (Lin) negative cells lacking expression of the follow markers: (CD3, CD5, NK1.1, CD27, TCRβ antibodies on the y-axis, B220, CD11b, CD11c antibodies on the *x*-axis). (**b**) Expression of cell surface markers on Lin^{-} CD90^{+} CD25^{+} lung ILCs in C57BL/6 WT (solid black line) and *Rag1*$^{-/-}$ mice (dashed black line) compared to isotype controls (gray shaded). (**a-b**) Data is representative of more than three experiments, *n* = at least 4 WT or *Rag1*$^{-/-}$ mice. (**c**) Absolute number of CD90^{+} CD25^{+} ILCs in naïve WT or *Rag1*$^{-/-}$ lung. **d**) Flow cytometry plots of pre-sort and post-sort purity of CD90^{+} CD25^{+} T1-ST2^{+} WT lung ILCs, gated on live, lineage negative cells. (**e**) IL-5 and IL-13 cytokine secretion from flow sorted CD90^{+} CD25^{+} T1-ST2^{+} lung ILCs cultured with IL-2 + IL-7 alone or in combination with IL-33 for four days, measured by ELISA. Data is representative of three independent experiments, *n* = 3 replicates, each replicate consisting of ILCs sorted from 5 pooled lungs. (**f**) Intracellular cytokine staining for IL-22 and IL-17A in Lin^{-} CD90^{+} CD25^{+} lung ILCs or spleen CD90^{+} CD4^{+} LTi cells from WT mice,

stimulated with 50 ng/ml rIL-23 (12 h) + PMA and Ionomycin (4 h). (**g**) IL-17A cytokine secretion from flow sorted $CD90^+$ $CD25^+$ T1-$ST2^+$ lung ILCs or spleen $CD90^+$ $CD4^+$ LTi cells cultured with IL-2 + IL-7 alone or in combination with IL-23 for four days, measured by ELISA. Data is representative of two independent experiments, $n = 3$ replicates, each replicate consisting of ILCs sorted from 3 pooled lungs or spleens. (**h**) Intracellular cytokine staining in Lin^- $CD90^+$ $CD25^+$ lung ILCs from WT mice treated with 500 ng rIL-33 for 7 days *in vivo* and stimulated with PMA + Ionomycin (4 hours) *ex vivo*. (**f,h**) Data is representative of 2 or more experiments, $n = 3$–4 mice.

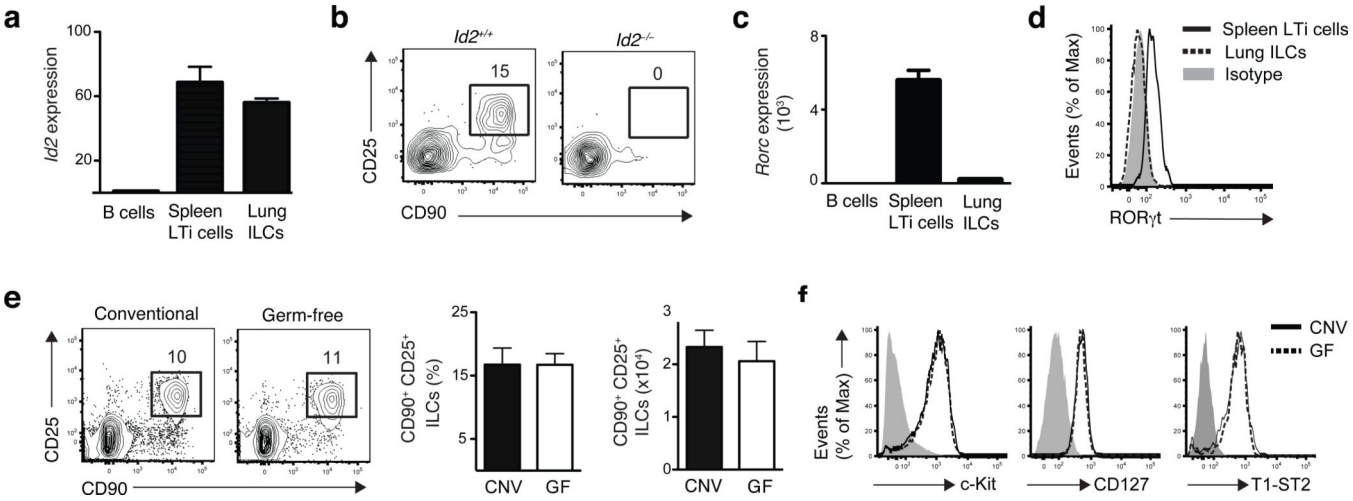

Figure 2. Development of lung ILCs requires Id2 but is independent of microbial signals

(**a,c**) mRNA expression of Id2 (**a**) or RORc (**c**) in sort purified Lin$^-$ CD90$^+$ CD25$^+$ lung ILCs and Lin$^-$ CD90$^+$ CD4$^+$ splenic LTi cells, normalized to β-actin and shown relative to expression levels in purified B220$^+$ B cells. *n* = 3 replicates, each replicate consisting of spleens (LTi cells) or lungs (ILCs) pooled from 5 C57BL/6 WT mice. (**b**) Flow cytometry plots of CD90$^+$ CD25$^+$ lung ILCs in WT or Id2-deficient bone marrow chimeras sacrificed 10 weeks post reconstitution, gated on live Lin$^-$ donor cells. Data is representative of 3 experiments, *n* = 2–4 *Id2*$^{+/+}$ or *Id2*$^{-/-}$ chimeras. (**d**) Flow cytometry plot of RORγt expression in CD90$^+$ CD25$^+$ lung ILCs (dashed black line) or CD90$^+$ CD4$^+$ LTi cells (solid black line) compared to isotype antibody control (gray shaded). (**e**) Representative flow cytometry plots, total frequency, and absolute cell number of lung Lin$^-$ CD90$^+$ CD25$^+$ ILCs in conventional C57BL/6 (CNV) or germ-free (GF) mice. (**f**) Cell surface expression of c-kit, CD127, and T1-ST2 on Lin$^-$ CD90$^+$ CD25$^+$ lung ILCs in CNV (solid black line) or GF (dashed black line) mice compared to isotype controls (gray shaded). (**e-f**) Data is representative of 2 independent experiments. Data shown are the mean ± SEM, *n* = 3–5 CNV or GF mice.

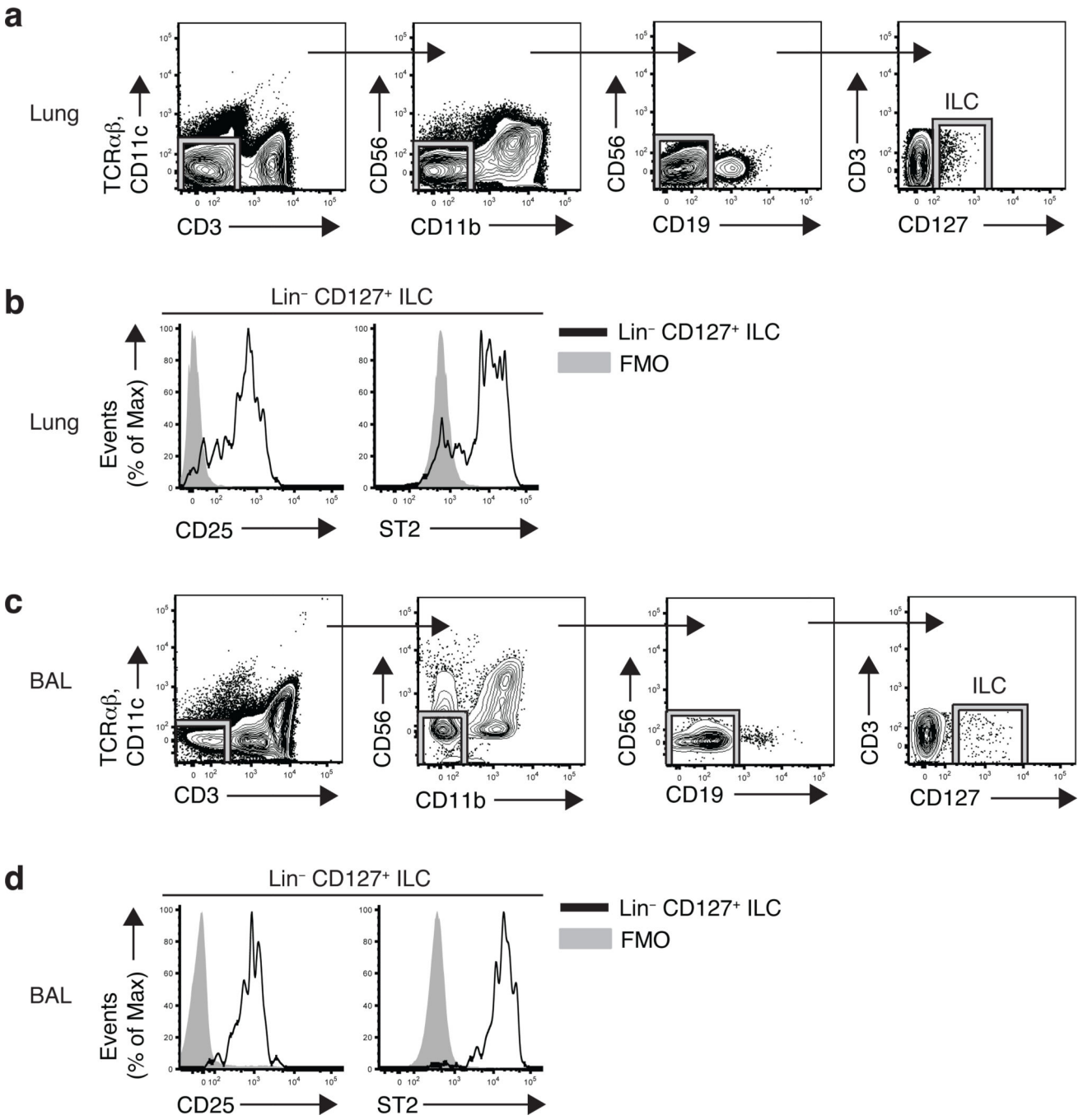

Figure 3. Lin$^-$ CD127$^+$ CD25$^+$ ST2$^+$ ILCs in human lung and airways

(**a,c**) Flow cytometric gating strategy for identifying CD127$^+$ Lin$^-$ ILCs (CD3$^-$ TCRαβ$^-$ CD11c$^-$ CD11b$^-$ CD19$^-$ CD56$^-$) in human lung parenchyma tissue (lower lobe) (**a**) or bronchoalveolar lavage (BAL) fluid (**c**), plots gated on live cells. (**b,d**) Expression of CD25 and ST2 on lineage negative CD127$^+$ human lung parenchyma cells (**b**) and BAL cells (**d**) (black line) compared to FMO controls (gray shaded). FMO = fluorescence minus one. For examination of human BAL, data shown is representative of 7 of 9 lung transplant recipient

patients examined. Data from lung parenchyma is representative of four cadaver tissue donors.

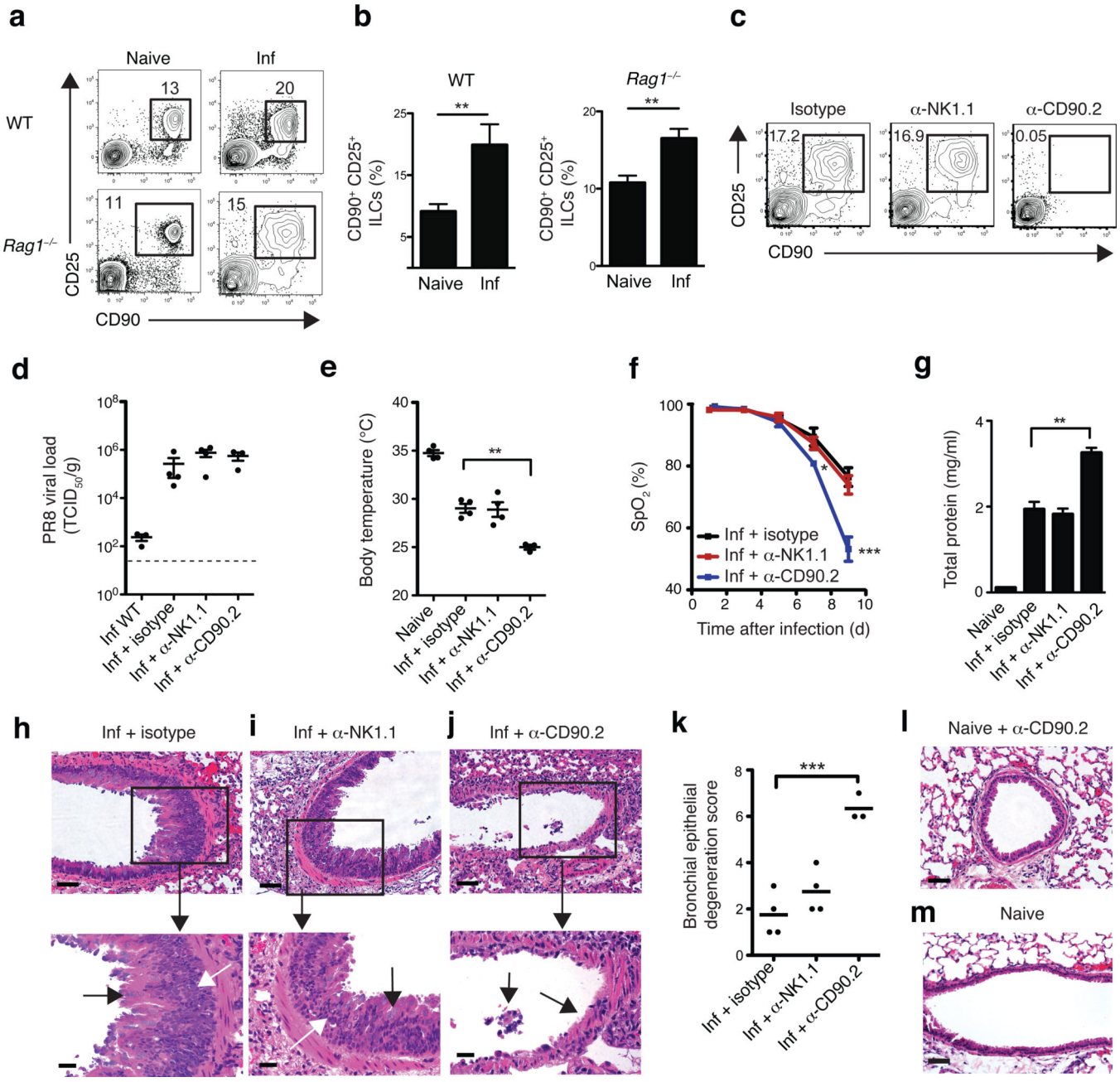

Figure 4. Depletion of CD90$^+$ ILCs during influenza infection results in reduced lung function, compromised epithelial integrity and impaired airway remodeling

Representative flow cytometry plots (**a**) and frequency (**b**) of Lin$^-$ CD90$^+$ CD25$^+$ ILCs in the lung parenchyma of naïve or intranasally infected (0.5 LD_{50} PR8) C57BL/6 WT mice (day 16 p.i.) and *Rag1*$^{-/-}$ mice (day 10 p.i.). (**c-k**) *Rag1*$^{-/-}$ mice were infected with 0.5 LD_{50} PR8 i.n. on D0 and treated with 200 μg of isotype, anti-NK1.1, or anti-CD90.2 mAb i.p. on D-1, D2, D5 and D8 p.i. and sacrificed day 10 p.i. (**c**) Representative flow cytometry plots of Lin$^-$ CD90$^+$ CD25$^+$ ILCs in the lungs of antibody-treated *Rag1*$^{-/-}$ at day 10 p.i. (**d**) PR8 viral copies per gram of lung tissue at day 10 p.i. from infected, untreated WT mice or from infected, antibody-treated *Rag1*$^{-/-}$ mice, measured by quantitative PCR and expressed

as $TCID_{50}$ per gram, dashed line = limit of detection. (**e**) Body temperature measured in naïve mice and infected *Rag1*$^{-/-}$ at day 10 p.i. (**f**) Percentage blood oxygen saturation (SpO_2) over the course of PR8 infection. (**g**) Quantification of total protein present in the bronchoalveolar lavage (BAL) fluid at day 10 p.i., (**h-j**) H&E staining of lung tissue from PR8-infected isotype (**h**), anti-NK1.1 (**i**), or anti-CD90.2 (**j**) treated *Rag1*$^{-/-}$ mice, day 10 p.i. Scale bar, 50 μm. (**h,i**) Black arrows indicate goblet cell hyperplasia and white arrows indicate epithelial cell hyperplasia. (**j**) Black arrows denote regions of epithelial shedding/necrosis within the bronchioles. (**k**) Histological score of respiratory epithelial degeneration. H&E stained lung sections from day 10 p.i. PR8-infected antibody-treated *Rag1*$^{-/-}$ mice were blindly graded on a scale of 0–10 for degree of bronchial/bronchiolar epithelial degeneration and necrosis. (**l-m**) H&E staining of lung tissue from anti-CD90.2 treated naive mice (**l**) and untreated naive mice (**m**). Scale bar = 50 μm. (**a-m**) Data is representative of 3 or more independent experiments n = 3–4 mice per group. Data shown are the mean ± SEM. * $P < 0.05$, ** $P < 0.01$, *** $P < 0.001$.

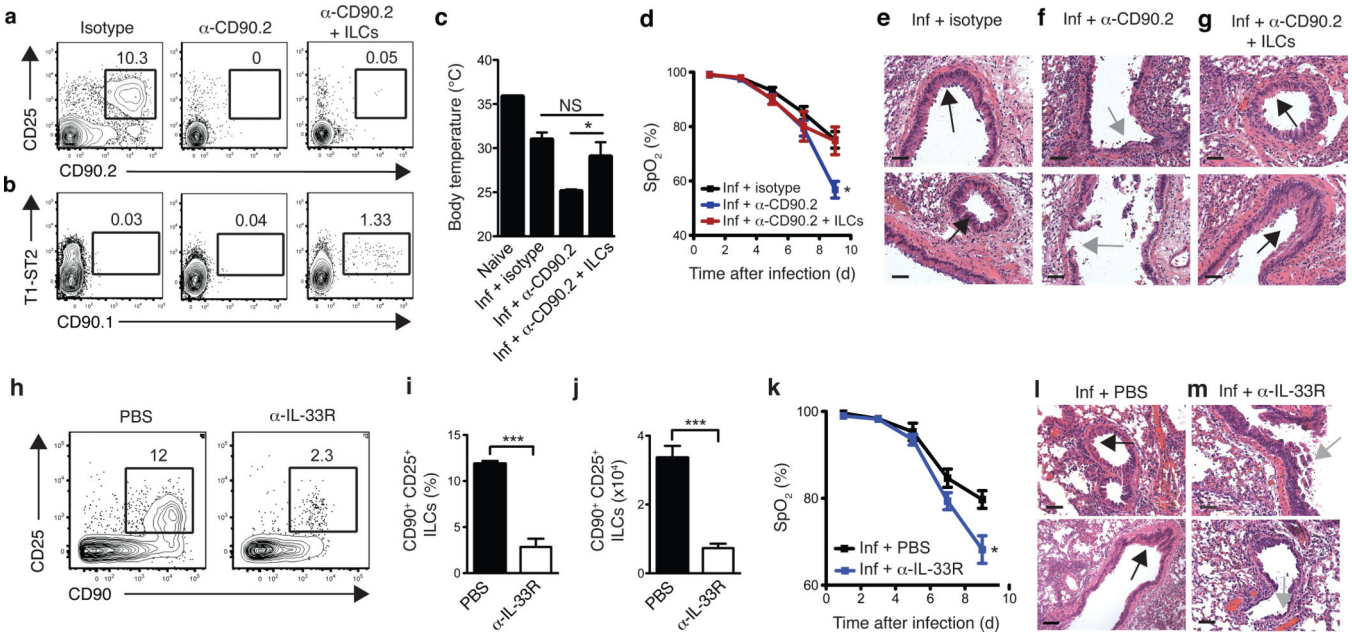

Figure 5. Adoptive transfer of lung-resident ILCs promotes tissue remodeling in anti-CD90.2-depleted mice while blockade of IL-33R signaling impairs lung function and airway repair

(**a-g**) *Rag1*$^{-/-}$ mice were infected with 0.5 LD_{50} PR8 i.n. on D0 and treated with 200 μg of isotype or anti-CD90.2 mAb i.p. on D-1, D2, D5, and D8 p.i. and sacrificed day 10 p.i. One group of anti-CD90.2-treated mice also received 1 × 10^5 FACS-sorted Lin$^-$ CD90.1$^+$ CD25$^+$ T1/ST2$^+$ lung ILCs i.v. at D0 and D5 p.i. (**a-b**) Flow cytometry plots of endogenous Lin$^-$ CD90.2$^+$ CD25$^+$ ILCs (**a**) and donor Lin$^-$ CD90.1$^+$ T1/ST2$^+$ ILCs (**b**) in the lungs of antibody-treated *Rag1*$^{-/-}$ at day 10 p.i.. (**c**) Body temperature measured in naïve mice and infected *Rag1*$^{-/-}$ at day 10 p.i. (**d**) Percentage blood oxygen saturation (SpO_2) over the course of PR8 infection. (**e-g**) H&E staining of lung tissue from PR8-infected isotype (**e**), anti-CD90.2 (**f**), or anti-CD90.2 + CD90.1 lung ILCs (**g**) treated *Rag1*$^{-/-}$ mice, day 10 p.i. Scale bar, 50 μm. Black arrows indicate epithelial cell hyperplasia and gray arrows denote regions of epithelial shedding/necrosis within the bronchioles. Scale bar = 50 μm. (**a-g**) Data is representative of 2 independent experiments n = 3–4 mice per group. (**h-m**) C57BL/6 WT mice received 200 μg anti-IL-33R (ST2) mAb or PBS every 3 days following infection with 0.5 LD_{50} PR8. Representative flow cytometry plots (**h**) and frequency and cell number (**i,j**) of CD90$^+$ CD25$^+$ ILCs in the lung of antibody-treated WT mice at 10 days p.i. (**k**) Pulse oximetry measurement of blood oxygen saturation levels. (**l-m**) H&E staining of lung tissue from PR8-infected PBS-treated mice (**l**) or anti-IL-33R-treated mice (**m**) at day 10 p.i. Black arrows indicate epithelial cell hyperplasia and gray arrows denote regions of epithelial shedding/necrosis within the bronchioles. Scale bar = 100 μm. Data is representative of 3 independent experiments *n* = 3–4 mice per group. Data shown are the mean ± SEM. * P < 0.05, ** P < 0.01, *** P < 0.001.

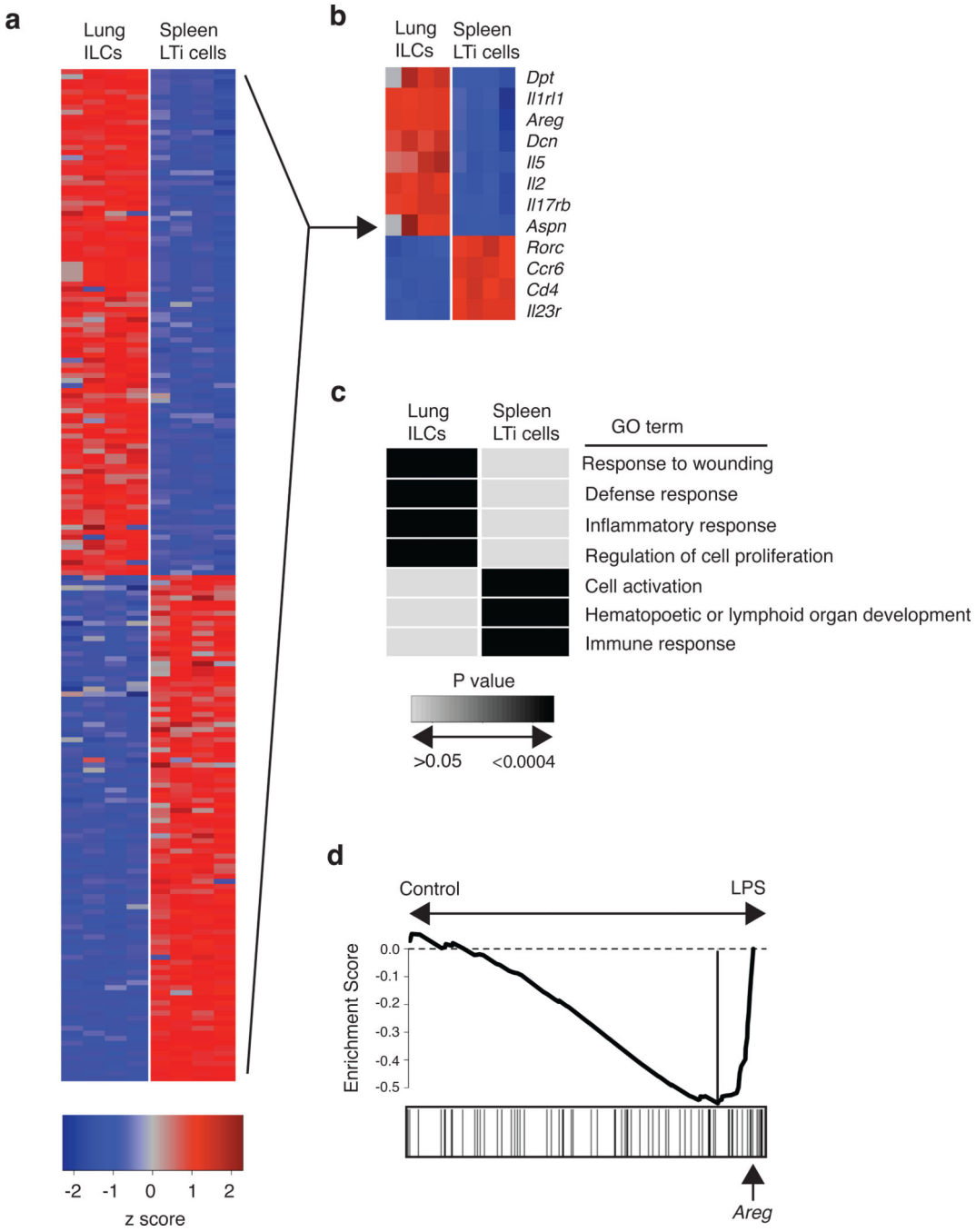

Figure 6. Global gene expression profiling of lung-resident ILCs reveals strong enrichment for genes regulating wound healing pathways

(**a-d**) CD90$^+$ CD25$^+$ ILCs and CD90$^+$ CD4$^+$ LTi cells were FACS-sorted from the lung (ILCs) or spleen (LTi cells) of naïve C57BL/6 WT mice. mRNA was isolated, amplified, and hybridized to Affymetrix gene chips for microarray analysis. (**a**) Heat map representing gene expression profiles of the top 100 differentially expressed genes in lung ILCs versus spleen LTi cells. Red = high expression, blue = low expression. (**b**) Heat map of key genes highly expressed in lung ILCs or spleen LTi cells. Red = high expression, blue = low

expression (**c**) Gene expression signatures of ILC and LTi cells (genes differentially expressed by two-fold or greater) were examined using Database for Annotation, Visualization and Integrated Discovery (DAVID) to identify enriched Gene Ontology terms describing biological processes. Shaded boxes represent significant enrichment (light gray $P > 0.05$, black $P < 0.0004$). (**d**) Gene Set Enrichment Analysis comparing the lung ILC gene expression signature with a previously published data set examining the effects of LPS-induced acute lung injury. Analysis of the top transcripts in the LPS-treated group shows presence of amphiregulin (highlighted by arrow).

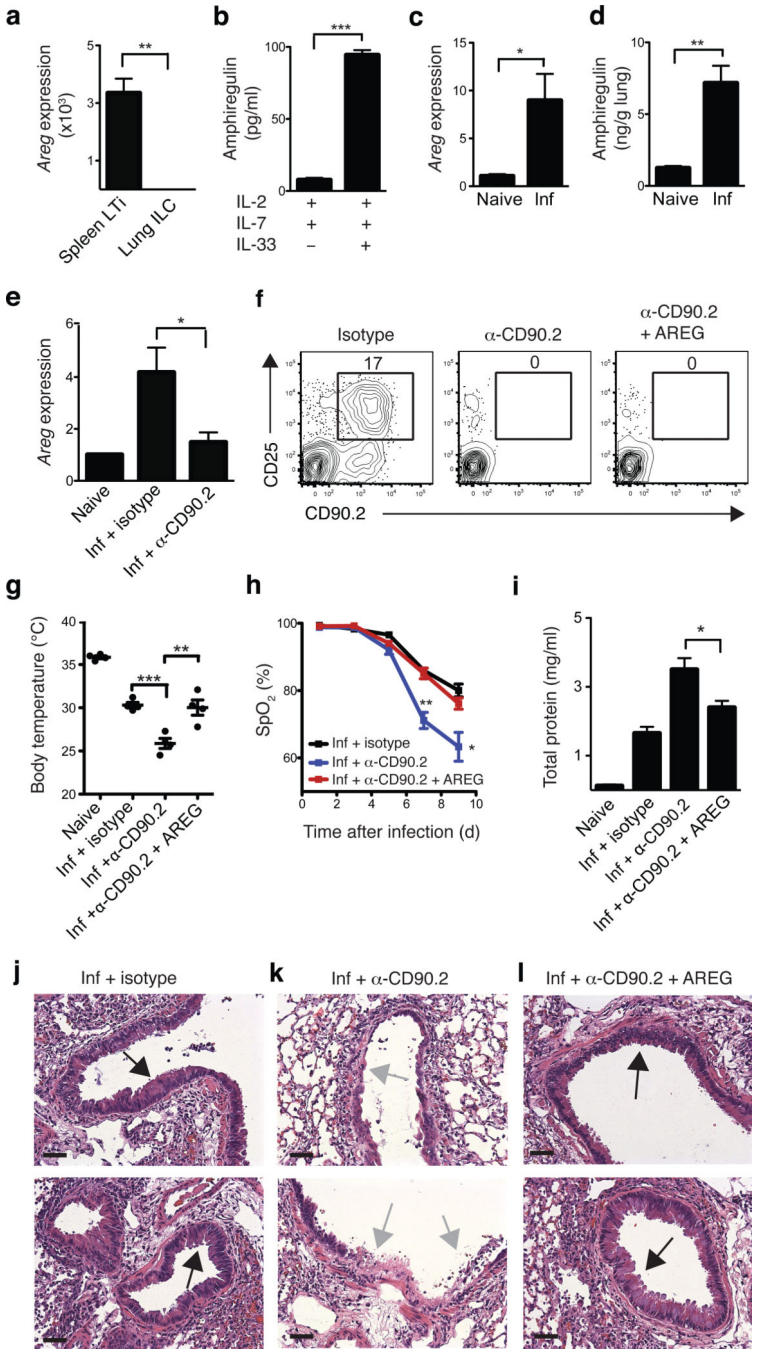

Figure 7. Amphiregulin is produced by lung ILCs and can restore lung function, barrier integrity and respiratory tissue remodeling following influenza virus-induced damage

(**a**) mRNA expression of amphiregulin (*Areg*) in sort-purified CD90$^+$ CD25$^+$ T1/ST2$^+$ lung ILCs compared to CD90$^+$ CD4$^+$ splenic LTi cells. (**b**) Production of amphiregulin protein by sort-purified lung ILCs stimulated with IL-2, IL-7, +/− IL-33 for four days, as measured by ELISA. mRNA (**c**) and protein (**d**) expression of amphiregulin in the lung of naïve or PR8-infected *Rag1*$^{-/-}$ mice at day 10 p.i. (**e**) mRNA expression of amphiregulin in the lung of naïve or PR8-infected *Rag1*$^{-/-}$ mice receiving isotype or anti-CD90.2 mAb (day 10 p.i.). (**f-**

l) *Rag1*$^{-/-}$ mice were infected i.n. with 0.5 LD_{50} PR8 and treated with isotype, anti-CD90.2 mAb, or anti-CD90.2 mAb + 5–10 μg recombinant murine amphiregulin i.p. every 2 days. (**f**) Representative flow cytometry plots of lung ILCs in antibody-treated mice. (**g**) Body temperature of antibody-treated mice at day 10 p.i. (**h**) Percentage blood oxygen saturation in antibody-treated mice. (**i**) Total protein concentration in BAL fluid at day 10 p.i. (**j-l**) H&E staining of lung tissue in isotype (**j**), anti-CD90.2 (**k**) and anti-CD90.2 + AREG (**l**) treated mice at day 10 p.i. Black arrows indicate epithelial cell hyperplasia and gray arrows denote regions of epithelial shedding/necrosis within the bronchioles. Scale bar = 50 μm. Data is representative of 2 independent experiments n = 3–4 mice per group. Data shown are the mean ± SEM. *$P < 0.05$, ** $P < 0.01$, *** $P < 0.001$.